Int. J. Heat Mass Transfer. Vol. 18, pp. 597–605. Pergamon Press 1975. Printed in Great Britain

IMPINGEMENT TRANSFER COEFFICIENTS DUE TO INITIALLY LAMINAR SLOT JETS

E. M. SPARROW and T. C. WONG
Department of Mechanical Engineering, University of Minnesota, Minneapolis, Minnesota, U.S.A.

(*Received* 9 *July* 1974)

Abstract—The transfer coefficients resulting from the impingement of a slot jet on a plane surface have been measured by the naphthalene sublimation technique. The experiments were performed with jets that are laminar at the exit of the duct from which the jet issues. In addition, the velocity profiles at the duct exit were fully developed. Distributions of the local mass-transfer coefficient on the impingement surface were determined for five Reynolds numbers and at five separation distances between the duct and the surface. The mass-transfer results can be converted to heat-transfer results by using the heat-mass transfer analogy.

It was found that the transfer coefficients generally tended to decrease with increasing separation distance, but there was evidence of non-monotonic behavior owing to the opposite influences of mixing-induced turbulence and diminished jet velocity. Increases in Reynolds number tended to increase the transfer coefficients, and the stagnation point values were correlated with a 0·6-power dependence. The surface distributions of the transfer coefficient were bell-shaped, with the largest value at the stagnation point. Comparisons with available literature suggested that the shape of the initial velocity profile has a significant effect on the transfer characteristics of the impingement surface.

NOMENCLATURE

- B, slot width;
- D_e, equivalent diameter, equation (4);
- $\mathscr{D}$, diffusion coefficient;
- H, distance between duct exit and impingement surface;
- K, mass-transfer coefficient, equation (2);
- $\dot{m}$, local mass-transfer rate/area;
- Nu, local Nusselt number, $Nu_B = hB/k$;
- Pr, Prandtl number;
- Re, Reynolds number at nozzle exit, $Re_D = \bar{u}D_e/\nu$, $Re_B = \bar{u}B/\nu$;
- Sc, Schmidt number;
- Sh, local Sherwood number, $Sh_D = KD_e/\mathscr{D}$, $Sh_B = KB/\mathscr{D}$;
- t_0, duration time of a data run;
- $\bar{u}$, mean velocity of jet at duct exit;
- x, y, surface coordinates, Fig. 1.

Greek symbols

- δ, sublimation depth;
- ν, kinematic viscosity;
- ρ_s, density of solid naphthalene;
- ρ_{nw}, concentration of naphthalene vapor at plate surface;
- $\rho_{n\infty}$, concentration of naphthalene vapor in the free stream.

INTRODUCTION

HEAT and mass transfer from surfaces in the presence of jet impingement is encountered in a wide range of industrial applications and has, therefore, been studied rather extensively. These studies have, in the main, been concerned with relatively high velocities so that the flow is turbulent at the exit of the nozzle from which the jet issues. The case of impingement heat or mass transfer with a jet that is laminar at the nozzle exit has received lesser attention. The present investigation is concerned with slot jets (i.e. two-dimensional jets) having such a laminar exit condition. Local transfer coefficients were measured on the impingement surface using a mass-transfer technique. Corresponding heat-transfer results can be deduced by employing the analogy between heat and mass transfer.

The experiments were performed by using the naphthalene sublimation technique. To employ the method, naphthalene plates were cast in a specially designed mold which, together with the casting technique itself, ensured that the plate surfaces would possess a high degree of smoothness and flatness. Painstaking measurements of the surface contour before and after a test run were made with a sensitive dial gage. The local changes in surface elevation and the duration time of the data run yielded the local transfer rates and these, when divided by the wall-to-stream concentration difference, gave the local transfer

coefficients. The results will be presented in dimensionless form in terms of the local Sherwood number. Air was the working fluid.

The slot-width Reynolds numbers of the experiments covered the range from about 150 to 950. At each Reynolds number, the distance between the jet exit and the impingement surface was varied from 2 to 20 times the slot width. The boundary condition for the experiments was uniform wall concentration of the naphthalene vapor, which corresponds, by analogy, to uniform wall temperature for the heat-transfer case.

In planning the research, careful consideration was given to the shape of the velocity profile at the nozzle exit. Previous work by Scholtz and Trass [1] for axisymmetric jets with laminar nozzle-exit conditions indicated that the transfer coefficients on the impingement surface were significantly different depending on whether the exit profile was flat or parabolic. For slot-jet impingement, the only available low Reynolds number experiments (Gardon and Akfirat [2]) appear not to have had a well defined exit velocity profile; but, if anything, the profiles were more flat than parabolic. To orient the present research so as to complement the available information on low Reynolds number slot-jet impingement, the apparatus was designed to provide a fully developed velocity profile at the nozzle exit.

In contrast to heat-transfer measurements, the use of the naphthalene sublimation technique offers a number of advantages for determining local transfer coefficients. Heat flux gages, besides being complex, are often of uncertain accuracy owing to extraneous losses, and their finite size does not permit truly local measurements to be made. Some gages require calibration, which introduces another degree of uncertainty. Furthermore, the attainment of a desired thermal boundary condition on the heat-transfer surface itself may be made difficult owing to extraneous losses and edge effects. With the naphthalene technique, highly local results are readily obtained by traversing the test surface with a sensitive depth indicator. The boundary condition of uniform wall concentration (analogous to uniform wall temperature) is attained when the test surface is isothermal.

Literature dealing with local transfer coefficients associated with the impingement of a slot jet will now be briefly reviewed. The earliest relevant publication unearthed by the authors was a company report by Daane and Pantaleo [3] that was cited in a later paper by Daane and Han [4]. In the Daane–Pantaleo experiments, heat-transfer rates were measured with the aid of a heated element embedded in micarta, but no mention was made of guard heating to prevent conduction losses nor was information given about the nozzle-exit Reynolds number. The paper by Gardon and Akfirat [2], which was cited above, provided local heat-transfer results for slot-width Reynolds numbers ranging from 450 to 22000, with the main emphasis being placed on Reynolds numbers in excess of those for laminar flow in the jet delivery nozzle. The measurements were made with an innovative heat flux gage. As noted in [2] (footnote 3, p. 107), the calibration may be a source of uncertainty. The naphthalene sublimation technique was employed by Korger and Krizek [5] and by Kumada and Mabuchi [6]. These investigators dealt with jets having slot-width Reynolds numbers on the order of 10000, which is more than an order of magnitude greater than the Reynolds numbers of the present study.

APPARATUS AND MEASUREMENT TECHNIQUE

The description of the experimental apparatus is facilitated by reference to Fig. 1. As shown there, air from the laboratory room is drawn through a rectangular duct and, at exit, becomes a slot jet which impinges on a naphthalene plate. The downstream end of the duct and the impingement plate are situated in a large test chamber. The impingement plate rests on a platform whose elevation can be varied, thereby providing a range of nozzle-to-plate separation distances. The air is withdrawn from the chamber through an aperture in the bottom wall, from where it is ducted to a flow meter, a blower, and finally to an exhaust system which is vented to the roof of the building.

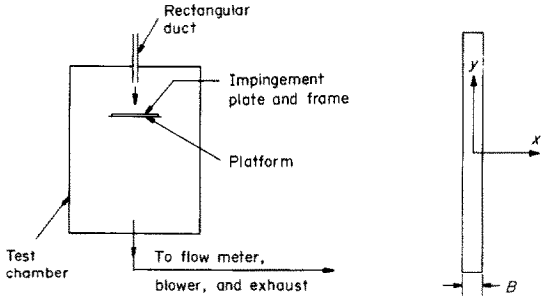

FIG. 1. Schematic of the experimental apparatus.

The use of a test chamber enabled the blower to be placed downstream of the impingement plate. The motivation for downstream positioning of the blower is to avoid preheating of the air which might have occurred had the blower been upstream. Since the vapor pressure of naphthalene is very sensitive to temperature (about 10 per cent variation per deg C at room temperature), preheating would have caused uncertainties in the results. The exhaust system ensured that the laboratory room was free of naphthalene vapor; the room itself was temperature controlled.

Therefore, the impinging jet was pure air of uniform and known temperature.

A rectangular duct was used to provide a slot jet with a fully developed laminar velocity profile at discharge. In designing the duct, the streamwise length required to develop the velocity distribution at the maximum anticipated Reynolds number was estimated from the analytical results of [7]. To provide a margin of safety, the design length of 48·3 cm (19 in) was chosen to be 50 per cent larger than the estimate based on [7]. The cross-sectional dimensions were 0·635 cm by 7·62 cm ($\frac{1}{4} \times 3$ in), which gave an aspect ratio of 12.

The test chamber was a metal tank, 1·52 m (5 ft) high with a 1·22 by 1·22 m (4 × 4 ft) square cross-section. The chamber was fitted on three sides with plexiglass windows to enable installation and removal of the naphthalene plates. The windows also facilitated the measurement of the separation distance between the duct exit and the exposed surface of the naphthalene plate as well as the perpendicular alignment of the duct relative to the surface. These operations were performed with the aid of a cathetometer capable of discriminating vertical distances to within 0·05 mm (0·002 in) and whose eye piece was equipped with perpendicular hairlines.

The naphthalene plates were cast in a mold whose metallic components, a stainless steel base plate and four aluminum bars, had been hand polished and lapped to a mirror finish. The bars were arranged on the base plate so as to enclose an area 5·7 × 8·9 cm ($2\frac{1}{4} \times 3\frac{1}{2}$ in). Plexiglass pieces, 0·95 cm ($\frac{3}{8}$ in) square by 1·27 cm ($\frac{1}{2}$ in) high, were placed in each corner of the enclosed space. The ultimate function of the plexiglass pieces was to serve as legs to support the naphthalene test plate and, to this end, the height dimensions of the pieces were made identical to within close tolerances by hand finishing operations.

Molten naphthalene was poured into the enclosure and allowed to solidify under natural cooling conditions. The solidified naphthalene plate was readily separated from the mold components by strategic hammer blows, subsequent to which the aluminum bars were reassembled around the plate in order to form a frame.

During the pouring process, the level of the molten naphthalene was maintained below the height of the plexiglass corner pieces. Therefore, subsequent to unmolding, when the naphthalene plate was oriented with the test surface facing upward, the plexiglass pieces became legs which supported the plate.

The naphthalene test surface was, of course, that which had been in contact with the base plate of the mold. The smoothness and flatness of the surface was such that no further finishing operations were needed. Furthermore, lubricants were never used to facilitate the removal of the plates from the mold. Each test plate was cast from fresh (i.e. unused) reagent grade naphthalene, and all implements associated with the casting process were kept scrupulously clean. The test surface was never touched subsequent to unmolding. In view of these procedures and precautions, it can be assumed with confidence that the test surfaces of the naphthalene plates were free of contamination. To ensure thermal equilibrium, the cast plate, sealed in plastic wrap, was left in the laboratory room overnight prior to a data run.

As indicated in Fig. 1, the naphthalene test plates were positioned on a platform. The platform was suspended from the top of the test chamber by four guide rods (not shown in the figure), one at each corner. Positioning holes in the guide rods enabled the platform to be fixed at discrete positions at distances from the duct exit ranging from 2 to 20 times the slot width. The platform itself was fabricated from aluminum tool plate, and its dimensions were 25·4 × 50·8 cm (10 × 20 in). A cardboard frame whose surface was flush with that of the test plate served to avoid flow separation of the air stream as it passed the downstream edge of the plate.

The contour of the naphthalene surface was measured both before and after a data run by a precision dial gage whose smallest scale division was 0·00005 in (~0·001 mm). The dial gage was mounted on a fixed strut that overhung a movable coordinate table. During the contour measurements, the naphthalene plate was held firmly against the coordinate table by flat springs. The position of the plate on the table was fixed by metal stops. The coordinate table provided two directions of horizontal travel and was equipped with micrometer heads from which the horizontal position could be read to 0·002 mm (~0·0001 in).

To ensure the accuracy of the mass-transfer results deduced from the surface contour measurements, it is mandatory that there be no extraneous differences in the elevations sensed by the dial gage before and after a data run. Potential errors in vertical positioning were eliminated by using selected locations on the upper exposed faces of the plexiglass legs as reference points. Surface contour measurements subsequent to a data run were not initiated until the elevations at the reference points were adjusted so as to be identical to those measured prior to the data run. The measured surface contours were slightly affected by natural convection sublimation which was operative during the period when the test plate was on the coordinate table and during the set-up of the experiment in the test chamber. Corrections to take account of the effect of natural convection will be discussed later.

Measurements of the flow rate were made with a calibrated rotameter, whereas the air temperature at the

duct exit was sensed by a calibrated 36-gage copper–constantan thermocouple in conjunction with a digital voltmeter. The various duration times needed to process the data were indicated by a digital timer.

ANALYSIS OF DATA

The local rate of mass transfer at any surface location can be evaluated from the local change of surface elevation in conjunction with the duration time of the respective data run. The change of elevation will be referred to as the sublimation depth δ. The local values of δ were determined by differencing the measured surface elevations before and after a data run, and then correcting for extraneous sublimation due to natural convection. The natural convection correction for each data run was obtained by measuring the change in elevation of a location on the plate surface which was covered during the duration of the run, but was uncovered during the measurement and set-up periods. The typical sublimation depths due to natural convection were found to be about 0·0025 mm (0·0001 in).

The duration time of a data run was selected so that the sublimation depth δ at the stagnation point of the impinging jet was about 0·05 mm (0·002 in). Depending on the jet Reynolds number, the duration times ranged from about 2000 to 7000 s.

If ρ_s denotes the density of solid naphthalene ($\rho_s = 1{\cdot}145$ [8]) and t_0 is the duration time of a data run, then the local rate of mass transfer $\dot{m}$ per unit surface area can be evaluated as

$$\dot{m} = \rho_s \delta / t_0. \tag{1}$$

Next, a local mass-transfer coefficient K can be defined in terms of $\dot{m}$ and of the difference between the concentrations of naphthalene vapor at the wall and in the free stream, ρ_{nw} and $\rho_{n\infty}$, respectively; so that

$$K = \dot{m}/(\rho_{nw} - \rho_{n\infty}). \tag{2}$$

In the present experiments, $\rho_{n\infty} = 0$. To obtain ρ_{nw}, the naphthalene vapor pressure corresponding to the wall temperature was evaluated from the Sogin correlation [9] and then the perfect gas law was applied. Inasmuch as the naphthalene test surface was isothermal, the wall concentration ρ_{nw} was uniform.

A dimensionless presentation of the transfer coefficients may be made in terms of the local Sherwood number Sh. Two definitions, based on different characteristic dimensions, will be used here.

$$Sh_D = KD_e/\mathscr{D}, \quad Sh_B = KB/\mathscr{D} \tag{3}$$

where $\mathscr{D}$ is the coefficient of mass diffusion. The characteristic dimensions D_e and B are, respectively, the equivalent diameter of the rectangular duct and the slot width. From the definition of the equivalent diameter, it follows that for an aspect ratio $AR = 12$

$$D_e = 2B[AR/(1+AR)] = 1{\cdot}85B \tag{4}$$

so that

$$Sh_B = 0{\cdot}542 Sh_D. \tag{5}$$

Thus, the two Sherwood numbers differ only by a multiplicative constant.

The Sherwood number results will be plotted as a function of the streamwise coordinate x measured along the surface of the impingement plate. The orientation of the x coordinate is illustrated in the right-hand diagram of Fig. 1. The 12:1 rectangle shown there is a projection of the duct cross-section on the test surface. The surface contour measurements were confined primarily to traverses in x along the line $y = 0$, that is, along the centerspan of the jet. Some traverses which were made off the centerspan (i.e. $y \neq 0$) to examine the role of edge effects will be discussed later.

The results are to be parameterized by the Reynolds number of the duct from which the jet issues. Once again, two Reynolds numbers will be employed according to the definitions

$$Re_D = \bar{u}D_e/\nu, \quad Re_B = \bar{u}B/\nu \tag{6}$$

with the inter-relation

$$Re_B = 0{\cdot}542 Re_D. \tag{7}$$

Re_B has already been referred to as the slot-width Reynolds number, whereas Re_D is the conventional duct Reynolds number.

The kinematic viscosity appearing in equation (6) was evaluated as that of pure air, taking cognizance of the minute concentrations of naphthalene vapor. The diffusion coefficient $\mathscr{D}$ is related to the Schmidt number via $\mathscr{D} = \nu/Sc$. The Schmidt number for the naphthalene–air system is 2·5 [9].

The mass-transfer results to be presented here may be converted to heat-transfer results by employing the heat–mass transfer analogy. According to the analogy, the conversion between the Sherwood and Nusselt number results at the same Reynolds number can be accomplished by the relation

$$Nu = (Pr/Sc)^n Sh \tag{8}$$

where n is usually $\frac{1}{3}$ or 0·4.

RESULTS AND DISCUSSION

Surface distributions

Distributions of the local mass-transfer coefficients on the impingement surface are presented in Figs. 2–4. In each figure, the local Sherwood number Sh_D is plotted as a function of the streamwise coordinate x, with $x = 0$ corresponding to the centerline of the impinging jet as illustrated in the right-hand diagram

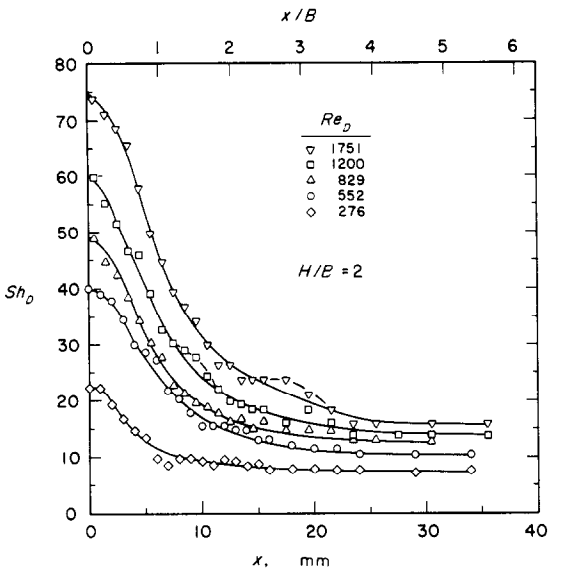

FIG. 2. Distributions of the local mass-transfer coefficient on the impingement surface, $H/B = 2$.

of Fig. 1. The streamwise coordinate itself is used on the lower abscissa scale, whereas the dimensionless coordinate x/B is used on the upper abscissa. Owing to symmetry about $x = 0$, results are shown only for $x \geqslant 0$. In each figure, the data are parameterized by the duct Reynolds number Re_D based on the hydraulic diameter D_e. The range of Re_D is from about 275 to 1750. The results can, if desired, be converted to the parameters Sh_B and Re_B by using equations (5) and (7).

The successive figures correspond to increasing values of the dimensionless separation distance H/B between the duct exit and the impingement surface (H is the separation distance and B is the slot width). Results for $H/B = 2$, for $H/B = 5$ and 10, and for $H/B = 15$ and 20 are respectively presented in Figs. 2–4. Actual data points are plotted in Fig. 2 along with faired curves to provide continuity. In Figs. 3 and 4, only the faired curves are shown in order to achieve a less cluttered presentation.

Attention may first be turned to Fig. 2. It is seen from the figure that for any fixed Reynolds number, the transfer coefficient decreases monotonically with increasing distance from the axis of impingement, with the distribution being bell-shaped. The solid lines defining the bell-shaped distributions were drawn as smooth curves. There are, however, small scale patterns in the data which suggest the presence of local humps in the distribution curves. Such humps are illustrated by the dashed lines for the two highest Reynolds numbers of the figure.

The general bell-shaped nature of the Sherwood number distributions is also in evidence in Figs. 3 and 4. In addition to the smooth curves (solid lines), dashed segments are also drawn in Fig. 3 to more closely follow the local variations of the data. Such variations could not be identified among the lower Reynolds numbers of Fig. 3. Similarly, the results for the cases represented in Fig. 4 did not display signs of humps in the distribution curves.

The general decrease of the local transfer coefficients with increasing distance from the impingement axis is a

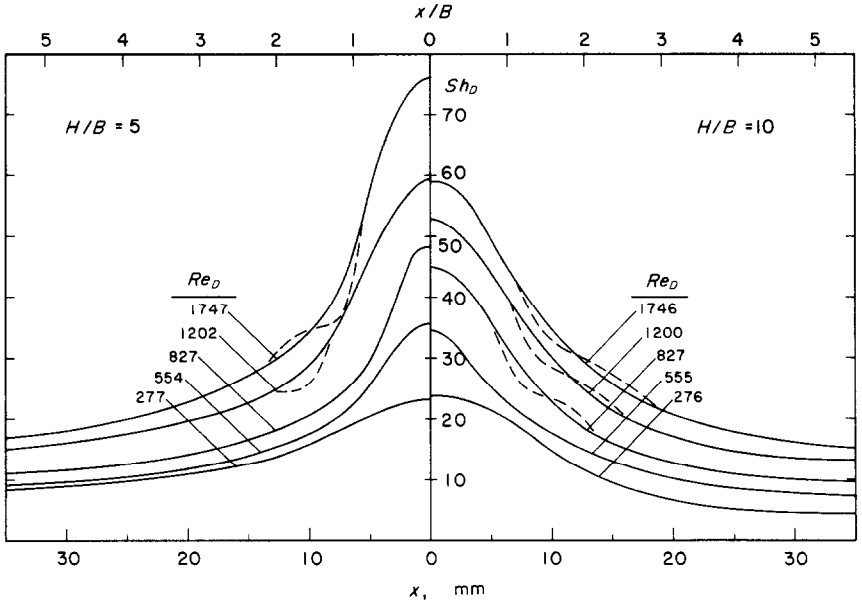

FIG. 3. Distributions of the local mass-transfer coefficient on the impingement surface, $H/B = 5$ and 10.

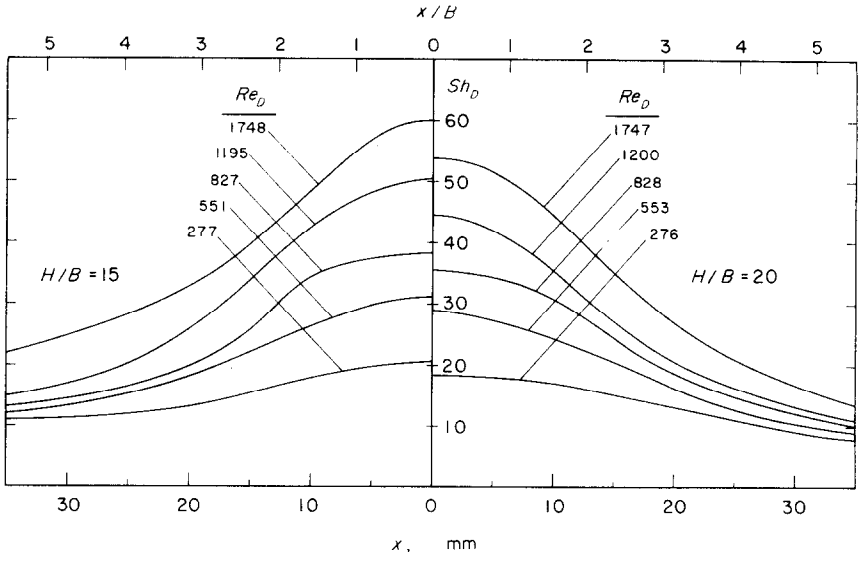

FIG. 4. Distributions of the local mass-transfer coefficient on the impingement surface, $H/B = 15$ and 20.

direct consequence of the thickening of the wall jet* which flows along the surface. The humps that appear in some of the distribution curves are symptomatic of a variety of complex phenomena that may be identified qualitatively but are not yet amenable to quantitative prediction.

One of these phenomena is the augmentation of boundary-layer heat or mass transfer in the presence of free stream turbulence and a streamwise pressure gradient. In the present problem, the free stream turbulence is generated by the mixing of the impinging jet with the quiescent environment, and the pressure gradient is induced by the deflection of the jet by the impingement plate. Another potentially relevant process is the laminar–turbulent transition of the wall jet, which may be decisively influenced by the turbulence level of the impinging jet itself, by the free stream turbulence level, and by the disappearance of the stabilizing streamwise pressure gradient downstream of the impingement region.

The role of these processes has been incisively discussed by Gardon and Akfirat [10]. Unfortunately, aside from two distribution curves in the low Reynolds number range, all of the experimental results employed by these authors to motivate and substantiate their models correspond to relatively high Reynolds numbers. Furthermore, owing to the sparsity of their low Reynolds number data, comparisons of the surface distributions of the transfer coefficient cannot be made.

*A wall jet is a flow which is bounded on one side by a wall and on the other side by an otherwise quiescent environment.

Effect of separation distance

Another trend apparently in evidence in Figs. 2–4 is a general diminution of the transfer coefficients with increasing separation distance between the duct exit and the impingement surface. This trend is examined in greater detail in Fig. 5, where the Sherwood number Sh_D at the axis of impingement ($x = 0$) is plotted as a function of the dimensionless separation distance H/B. The data are parameterized by the duct Reynolds number Re_D. In accordance with usual practice, the $x = 0$ location on the impingement plate will hereafter be referred to as the stagnation point.

Inspection of the figure reveals that the dependence of the stagnation point transfer coefficient on the separation distance is by no means elementary and, depending on the Reynolds number, may not be monotonic. The trends are reflective of the complex processes which occur within the jet both prior to and at impingement. These processes will now be briefly reviewed.

Upon its emergence from the supply duct, the outer layers of the jet stream entrain (and are retarded by) fluid from the quiescent environment, thereby setting up a mixing zone characterized by strong turbulence. The inner layers of the jet stream, the so-called core, are not directly involved in the mixing process. The mixing zone progressively eats away the core, ultimately engulfing it.

The turbulence generated by the mixing process will depend on the velocity gradients associated with the entrainment. In the present problem, where the emerging jet has a parabolic velocity profile, one would

expect a less violent mixing than would occur for a jet having a flat velocity profile at the same Reynolds number. On the other hand, the situation may reverse during the later stages of mixing, when the relatively higher velocities in the central region of the parabolic profile begin to influence the entrainment process.

For free jets, it is usually assumed that the magnitude of the velocity in the core remains unchanged until the core is engulfed by the mixing zone. Thereafter, the centerline velocity decreases monotonically as the jet grows progressively broader. In the present problem, owing to the initially nonuniform velocity profile, there may be a readjustment in the core velocity distribution owing to the action of viscosity.

As the jet approaches the impingement surface, the deflection of the flow sets up pressure gradients. These pressure gradients can amplify the effects of the turbulence generated in the mixing region.

On the basis of the foregoing discussion, one can identify a number of factors which can influence the variation of the stagnation point transfer coefficients with separation distance. For small separations, it is likely that the core velocity will be independent of the separation distance, and the transfer coefficients should show a corresponding trend. Once the core has been engulfed by the mixing region,* the diminution of the centerline velocity would tend to bring about a decrease in the transfer coefficient, but turbulence generated by the mixing process would have an opposite effect. At the lower Reynolds numbers the former should be the decisive factor, whereas at the higher Reynolds numbers the turbulence should have some influence. These conflicting factors are probably responsible for the shapes of the curves of Fig. 5.

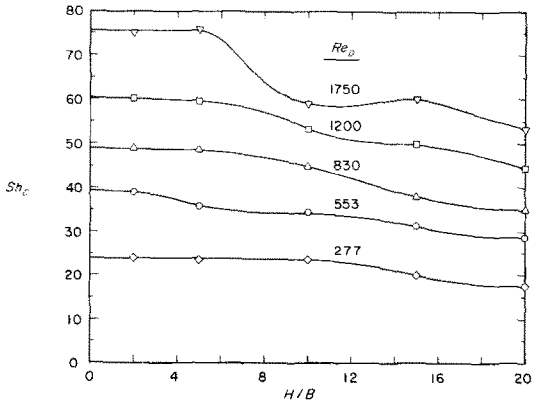

FIG. 5. Stagnation point transfer coefficients as a function of duct-to-surface separation distance.

*Albertson and co-workers [11] found that the core ended at about $H/B = 5$ when $Re_B = 1500$ with a flat initial velocity profile. Apparently, velocity information is not available for slot jets having lower Reynolds numbers and/or for nonuniform initial velocity profiles.

Gardon and Akfirat [10] have discussed in detail the flow phenomena which affect the stagnation point transfer coefficients. Their models were based on an initially flat velocity profile and on velocity field results at higher Reynolds numbers.

It is interesting to compare the present stagnation point results with those from the three low Reynolds number runs of Gardon and Akfirat [2, 10]. For this purpose, it was necessary to rationalize the difference between the present Schmidt number of 2·5 and the Prandtl number of 0·7 for the heat-transfer experiments. The rationalization was accomplished using equation (8) with $n = 0{\cdot}4$, the present Sherwood number results being converted to Nusselt numbers.

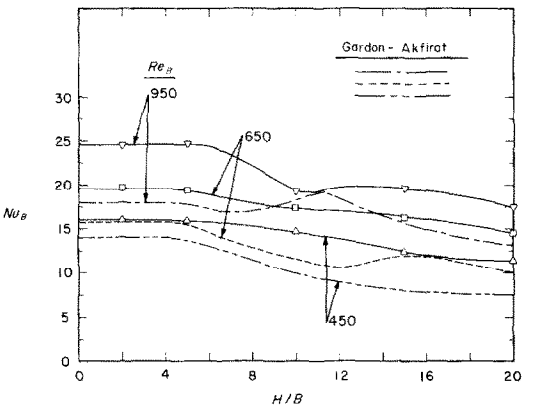

FIG. 6. Comparisons of stagnation point results.

The comparison is shown in Fig. 6, where Nu_B and Re_B are used to be consistent with the variables employed by Gardon and Akfirat. There are two features of this figure that are worthy of note. First, the Gardon–Akfirat results are non-monotonic at the two higher Reynolds numbers, which is consistent with the behavior at the highest Reynolds number of the present investigation. The fact that there are differences in the detail of the non-monotonic behavior is easily rationalized, since the relative importance of the factors which contribute to this behavior is different in the two experiments.

The other noteworthy aspect of the comparison is that the present results are about 30 per cent higher than those of Gardon and Akfirat. The main cause of this difference is the nature of the initial velocity profiles of the two investigations. In the present case, the fully developed velocity profile has a maximum value of 1·58 relative to $\bar{u}$,* whereas it was likely that the profile of [2, 10] was more flat than peaked. For low Reynolds number circular impinging jets, Scholtz

*From a solution for the 12:1 rectangular duct.

and Trass [1] have shown that the differences between a flat and a parabolic velocity profile can lead to a deviation in the stagnation point transfer coefficients of a factor of two.

Another (probably lesser) factor in the comparison is the finite size of the heat flux probe used in [2, 10]. It can be readily understood that such a probe, when centered at the point of maximum transfer coefficient, indicates a lower value because it averages over a finite distance.

Effect of Reynolds number

According to Figs. 2–4, the transfer coefficients increase with increasing Reynolds number. With a view to correlating the effect of Reynolds number, consideration was given to the grouping Sh_D/Re_D^m. Laminar boundary-layer theory suggests that $m = 0{\cdot}5$ at the stagnation point, but it is known that the effect of free stream turbulence can be appreciable and thereby cause deviations from the theoretical predictions.

To illustrate the outcome of the correlation effort, results are presented for $H/B = 5$ and 20 in Figs. 7 and 8. The quantities $Sh_D/Re_D^{0{\cdot}6}$ and $Sh_D/Re_D^{0{\cdot}5}$ are plotted in the upper and lower graphs of each figure against a dual abscissa which includes both x and x/B. The use of a logarithmic abscissa was purposeful in that it enlarges the impingement region. A linear scale was appended between $x = 0$ and $x = 1$ mm to accommodate the stagnation point data.

Examination of Figs. 7 and 8 indicates that the $Sh_D/Re_D^{0{\cdot}6}$ group is highly effective in bringing together the data at the stagnation point and in an adjacent portion of the impingement surface. Indeed, for the

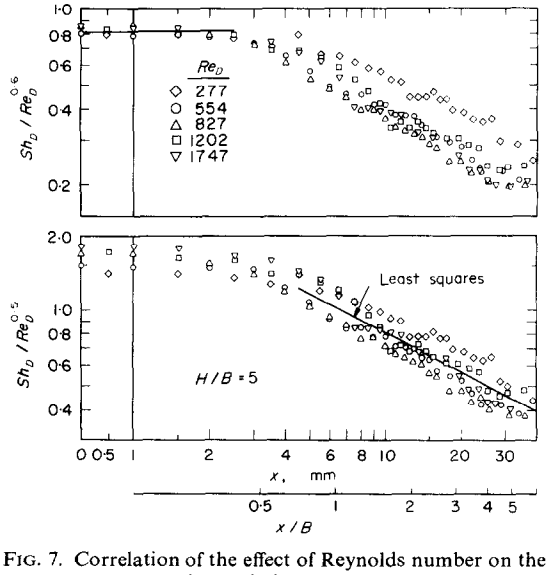

FIG. 7. Correlation of the effect of Reynolds number on the transfer coefficients, $H/B = 5$.

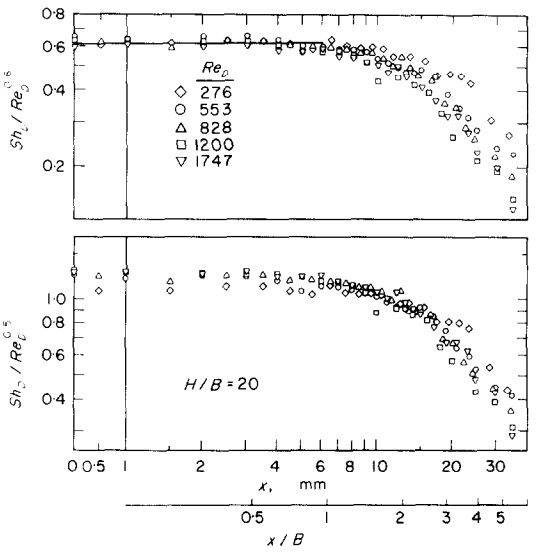

FIG. 8. Correlation of the effect of Reynolds number on the transfer coefficients, $H/B = 20$.

range of x/B where $Sh_D/Re_D^{0{\cdot}6}$ correlates the Reynolds number effect, it is also true that $Sh_D/Re_D^{0{\cdot}6}$ is independent of x/B. Comparison of Figs. 7 and 8 shows that the range of x/B where $Sh_D/Re_D^{0{\cdot}6}$ is constant increases with the separation distance. It is interesting to note that Gardon and Akfirat correlated their stagnation point results for high Reynolds number jets ($Re_B > 2000$) with the 0·58 power of the Reynolds number.

At larger values of x/B, in the wall jet region, neither $Sh_D/Re_D^{0{\cdot}6}$ nor $Sh_D/Re_D^{0{\cdot}5}$ is an effective correlation of the Reynolds number effect. The spread of the data may be slightly less for the latter grouping. A least squares straight line was put through the data in the lower part of Fig. 7 in order to obtain an estimate of the dependence on x/B, the result being $(x/B)^{-0{\cdot}51}$. Insufficient data were available in the wall jet region for $H/B = 20$ (Fig. 8) to warrant an x/B correlation.

Other remarks

Some consideration was given to assessing whether the present experiments fulfilled the objective of providing results for a slot jet, without significant end effects. To this end, the fully developed laminar velocity distribution for a 12:1 rectangular duct was evaluated. The velocity field was found to be spanwise uniform within $\frac{1}{3}$ per cent over 70 per cent of the span. In addition, some mass-transfer measurements were made for $y \neq 0$, that is, off the center-span. For instance, for $H/B = 10$ and $Re_D = 830$, measurements along the lines $y = 0$, $y = 7{\cdot}5$ mm, and $y = 15$ mm indicated only a slight fall-off of the data with increasing y (the half span dimension is 38·1 mm). At $x = 0$, there was virtually no fall-off with increasing y.

A graph showing the just-mentioned data relating to the spanwise effect is available in [12]. Also available in [12] are more detailed versions of Figs. 3 and 4, and plots similar to Figs. 7 and 8 for $H/B = 2$, 10, and 15.

REFERENCES

1. M. T. Scholtz and O. Trass, Mass transfer in a non-uniform impinging jet, *A.I.Ch.E. Jl* **16**, 82–96 (1970).
2. R. Gardon and J. C. Akfirat, Heat transfer characteristics of impinging two-dimensional air jets, *J. Heat Transfer* **88**, 101–108 (1966).
3. R. A. Daane and P. F. Pantaleo, Impingement air drying, Beloit Iron Works Report (April 1969).
4. R. A. Daane and S. T. Han, An analysis of air impingement drying, *Tappi* **44**, 73–80 (1961).
5. M. Korger and F. Krizek, Mass-transfer coefficient in impingement flow from slotted nozzles, *Int. J. Heat Mass Transfer* **9**, 337–344 (1966).
6. M. Kumada and I. Mabuchi, Studies on the heat transfer of impinging jet, *Bull. J.S.M.E.* **13**, 77–85 (1970).
7. E. M. Sparrow, S. H. Lin and T. S. Lundgren, Flow development in the hydrodynamic entrance region of tubes and ducts, *Physics Fluids* **7**, 338–347 (1964).
8. *Handbook of Physics and Chemistry*, p. C-414. Chemical Rubber Publishing Co., Cleveland, Ohio (1966–1967).
9. H. H. Sogin, Sublimation from disks to air streams flowing normal to their surfaces, *Trans. Am. Soc. Mech. Engrs* **80**, 61–71 (1958).
10. R. Gardon and J. C. Akfirat, The role of turbulence in determining the heat-transfer characteristics of impinging jets, *Int. J. Heat Mass Transfer* **8**, 1261–1272 (1965).
11. M. L. Albertson, Y. B. Dai, R. A. Jensen and H. Rouse, Diffusion of submerged jets, *Trans. Am. Soc. Civil Engrs* **115**, 639–664 (1950).
12. T. C. Wong, Mass transfer in an impinging jet, Thesis, Department of Mechanical Engineering, University of Minnesota, Minneapolis, Minnesota (1974).